Article

Hydroconversion of Waste Cooking Oil into Green Biofuel over Hierarchical USY-Supported NiMo Catalyst: A Comparative Study of Desilication and Dealumination

Zongwei Zhang [1,2] [iD]**, Qingfa Wang [1,*]** [iD]**, Hao Chen [1] and Xiangwen Zhang [1,*]**

[1]   Key Laboratory of Green Chemical Technology of Ministry of Education, School of Chemical Engineering and Technology, Tianjin University, Tianjin 300072, China; zhv116@163.com (Z.Z.); chen26352857@126.com (H.C.)

[2]   Airport Department, Civil Aviation University of China, Tianjin 300300, China

*   Correspondence: qfwang@tju.edu.cn (Q.W.); zhangxiangwen@tju.edu.cn (X.Z.); Tel./Fax: +86-22-2789-2340 (Q.W. & X.Z.)

Abstract: The hydroconversion of waste cooking oil into hydrocarbon fuel was investigated over the hierarchical USY zeolite-supported NiMo catalysts which were prepared by dealumination ($(NH_4)_2SiF_6$)/desilication (NaOH). The physical and acidity properties of the hierarchical catalysts were characterized by X-ray diffraction (XRD), the Brunauer-Emmett-Teller (BET) infrared spectroscopy of adsorbed pyridine (Py-IR), ammonia temperature-programmed desorption (NH_3-TPD), and H_2 temperature-programmed reduction (H_2-TPR). The Brønsted/Lewis (B/L) acid distribution was little affected by dealumination and the acid density decreased significantly. However, the highly-desilicated catalysts decreased the B/L ratio obviously. Therefore, many more Mo species in the $NiMoO_4^-$ and MoO_3 phases were produced in the AHFS-treated catalysts, while more high-valence-state Mo species in the $NiMoO_4^-$ phase were formed in the NaOH-treated catalysts. The AHFS-treated catalysts showed higher catalytic activity and better DCO_2 selectivity and selective cracking for jet fuel. The 42.3% selectivity of jet fuel and 13.5% selectivity of jet-range aromatics was achieved over the 8 wt % $(NH_4)_2SiF_6$-treated catalyst with 67% DCO_2 selectivity.

Keywords: waste cooking oil; hydroconversion; bio-jet fuel; dealumination; desilication

1. Introduction

The development of renewable fuels resources has received great attention because of the global environmental concern and the exhaustion of the fossil fuel resources [1–3]. The high demand of jet fuel has made the research of bio-jet fuel significant because of the rapid development in the aircraft industry and the compulsory reduction of carbon emissions. Hydroconversion of vegetable oils to obtain bio-jet fuel was a potential processing route [4–9]. Several routes based on hydrotreating of vegetable oil have been performed to produce aviation biofuels from biomass feedstocks. Among these routes, two-step processes are industrially available. Hydrodeoxygenation (HDO) is firstly employed to produce long-chain paraffins, followed by a hydroisomerization-hydrocracking to improve the cold properties and to obtain the desired chain length in another reactor. For example, the UOP Renewable Jet Fuel Process[TM], the Nesto Oil NEXBTL process, and Haldor Topsoe's HydroFlex[TM] technology have been developed to convert vegetable oil (jatropha oil, palm oil, etc.) into green jet fuel based on commercial Ni-based catalysts [10,11]. Recently, many works have been conducted to develop a one-step process to prepare bio-jet fuel from lipids. In these cases, HDO and hydroisomerization-hydrocracking occurred in a reactor. Sinha and co-workers [12] investigated the bio-jet fuel production from jatropha oil

by a single-step route using hierarchical ZSM-5-supported NiMo or NiW catalysts. A high yield of jet-ranged (C_9–C_{15}) hydrocarbons with excellent isomerization selectivity was obtained (40–45% with i/n = 2–6 and 40–50% with i/n = 3–13 over NiW and NiMo catalysts, respectively). The product distribution (jet fuel with desired aromatics, diesel, and gasoline) was tailored by the sulphided NiMo and NiW catalysts supported on hierarchical mesoporous SAPO-11 [13].

Generally, waste cooking oil is 2–3 times cheaper than vegetable oils [14,15] and has become a promising feedstock in biodiesel production [16–18]. However, very few works have been performed producing renewable jet fuel from WCO. Cheng's group [19] investigated three types of zeolites (Meso-Y, SAPO-34, and HY) loaded with nickel to convert waste cooking oil into bio-jet fuel. Zeolite Meso-Y exhibited a high yield of C_8–C_{16} alkane and a low aromatic yield from waste cooking oil. Hence, the research for new approaches to produce jet fuel from WCO is significant for academic research and potential industrial application.

Hierarchical zeolite showed excellent activity for the hydroconversion of lipids to hydrocarbons [12,13,19,20]. Recently, dealumination [21–23] and/or desilication [24–26] has been used as a versatile method to prepare the hierarchical zeolite. Many works have been done to regulate the pore structure and the surface acidity by these methods [22–26]. Although some work has compared the catalytic performance of desilicated and dealuminated zeolites in hydrodeoxygenation of vegetable oils. However, the nature of these methods on their catalytic activity is rarely involved. Moreover, owing to the significant relevance of zeolite Y to industrial catalysis, USY zeolite has been widely used as an acid catalyst in fluid catalytic cracking and hydrocracking because of its strong acidity and high hydrothermal stability [27]. However, despite the supremacy of Y zeolites in petroleum refining, diffusion limitations were recognized as a major problem that needed to be resolved to unleash its full potential. Therefore, in this work, the dealumination and desilication of the USY zeolite were investigated by $(NH_4)_2SiF_6$ (AHFS) and NaOH leaching, respectively. The catalytic activity of these modified zeolites was evaluated by converting WCO into biofuel. The object is to understand the role of desilication and dealumination on tuning the properties of the pore structure and the acidity distribution for its catalytic hydrodeoxygenation of WCO and, furthermore, to provide some sights for rational design of new hierarchical zeolite in WCO conversion.

2. Results and Discussion

2.1. Textural Structures of Desilicated and Dealuminated USY Zeolites

Table 1 shows the structure variation of modified USY zeolite by desilication and dealumination. The unit cell size of AHFS-dealuminated USY (AHFS-Y) gradually decreased with the acid treatment due to the removal of the longer Al-O band in the zeolite. Consequently, the Si/Al ratio increased. However, after desilication, the unit cell size of NaOH-treated USY increased and the Si/Al ratio decreased due to the removal of silicon. Obviously, the relative crystallinity of dealuminated and desilicated USY decreased dramatically. Moreover, the dealuminated catalysts of 4AHFS-Y and 8AHFS-Y showed similar relative crystallinity with the desilicated catalysts of 1NH-Y and 4NH-Y, respectively. Thus, these catalysts were further investigated. As for the parent USY and desilicated USY zeolites, the framework silicon-to-aluminum ratios determined by X-ray diffraction (XRD) (Si/Al_{XRD}) was lower than the bulk silicon-to-aluminum ratio determined by XRF, indicating the presence of a large amount of extra-framework silicon [22,25]. This suggests that the extra-framework silicon was easier to remove or part of exfoliated silicon recrystallized in the alkali-treatment [22,25,26].

After AHFS-dealumination, the framework Si/Al ratio significantly increased with a slight increase of bulk Si/Al ratio, and it was obviously beyond the bulk Si/Al ratio for the samples treated with high AHFS concentration (8AHFS-Y and 12AHFS-Y). This strongly suggested that the framework aluminum was mainly removed and the majority of extracted framework aluminum (FAL) turned into extra-framework aluminium (EFAL) in the AHFS treatment [28,29]. This was because the HF

acid produced from excessive AHFS destroyed the framework of USY and the vacancies created by dealumination increased [30,31].

Table 1. Crystal structure parameters of modified USY.

Sample	a_o (A)	Si/Al$_{XRD}$	Si/Al$_{XRF}$	Relative Crystallinity (%)
USY	24.515	4.1	8.8	100
4AHFS-Y	24.394	7.2	8.9	49
8AHFS-Y	24.247	28.8	10.2	37
12AHFS-Y	24.246	29.3	12.3	17
1NH-Y	24.485	4.7	6.6	50
4NH-Y	24.547	3.7	4.9	31

2.2. Acidity Distribution of Desilicated and Dealuminated USY

The acidity properties of samples were investigated by Py-FTIR and NH_3-TPD. From Figure 1, it could be observed that two NH_3 desorption peaks were detected in the range of 150–300 °C and 300–550 °C, which were assigned to weak and strong acidity, respectively. These peaks were deconvoluted (see Figure S1) and the acidity distribution calculated according to the amount of desorbed NH_3 was summarized in Table 2. The USY zeolite showed a high B/L ratio (2.92), indicating that USY was dominated by Brønsted acidity. The amounts of Brønsted acid and Lewis acid sites decreased with the increase of AHFS concentration due to the removal of framework Al, the Brønsted acid site. However, the AHFS-treated catalysts showed the similar B/L ratio indicating that dealumination had little influence on the distribution of Brønsted and Lewis site. The amount of strong acid sites increased under mild AHFS treatment (4 wt %) because of the superacidity of amorphous SiO_2-Al_2O_3 or EFAl formed after dealumination [21,28].
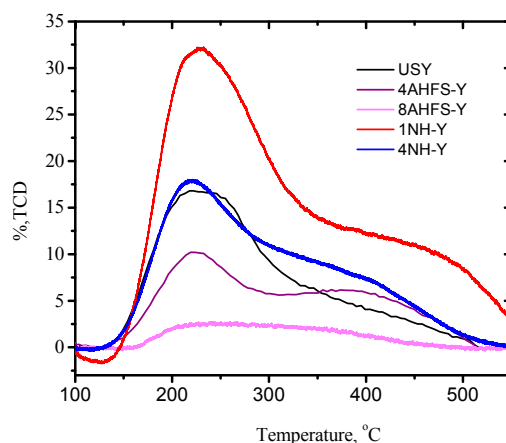

Figure 1. NH_3-TPD profiles of AHFS- and alkaline-treated USY.

Table 2. Acidity properties of samples (µmol/g).

Sample	B	L	Weak Acidity	Strong Acidity	B/L
USY	1851	634	626	660	2.92
4AHFS-Y	1440	483	402	857	2.98
8AHFS-Y	160	55	66	230	2.91
1NH-Y	2374	602	1545	1518	3.94
4NH-Y	1604	1254	658	1130	1.28

The weak acidity and strong acidity of alkali-treated USY were much larger than the parent one due to the increase of Al content in the zeolites. The amount of Brønsted acidity of 1NH-Y sample

significantly increased, probably due to the reinsertion of aluminum species to vacancies by silicon removal [22]. The 4NH-Y sample showed higher Lewis acid sites density because of the large part of FAL transform into EFAL. Therefore, the 1NH-Y sample showed a high B/L ratio (3.94), but a lower B/L ratio (1.28) for the 4NH-Y sample.

2.3. Pore Size Distribution of Treated USY Zeolites

The N_2 adsorption-desorption isotherms and pore size distributions using the NLDFT (non-local density functional theory) model are illustrated in Figure 2. The porous properties and the hierarchy factor (HF) values of all the catalysts are summarized in Table 3. The mesopore volume and the HF value increased considerably as the concentration of AHFS or NaOH increased, indicating that the introduction of mesopore reduced the micropore volume. From the pore size distribution profiles the peaks of AHFS treated samples shifted to the right and the intensities strengthened, indicating that the size and the amount of the mesopores increased. This indicates that the formation of secondary mesopores was closely related to the dealumination method and the mechanism of filling aluminium vacancies by silicon. The silicon insertion rate was too slow to repair the vacancies left by aluminum removal and mesopores formed, and the integrity of the zeolite framework may not be preserved [26]. Thus, with the increase of the mesopores' volume, the crystallinity declined (Table 1). The formation of the mesopores on the subsurface of the dealuminated USY also reduced the surface acidity (Tables 2 and 3) [26]. Moreover, the catalysts treated by 8% AHFS and 4% NaOH showed the comparable HF values. Much higher concentration of AHFS (12%) would damage part of the formed mesopore leading to the decrease of HF value. As shown in Figure 2, the dealuminated catalysts by highly-concentrated AHFS (8% and 12%) showed a high content of mesopores. However, the desilicated catalysts produced much bigger mesopore size than dealuminated catalysts (20–30 nm vs. 12–15 nm).
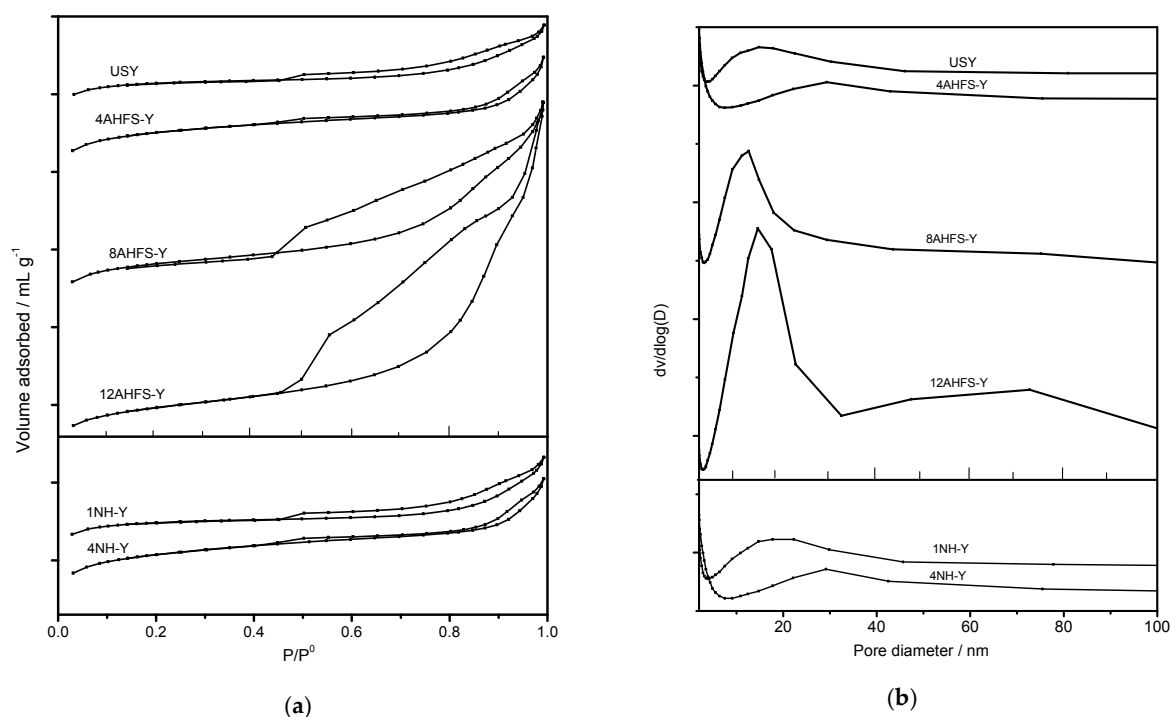

Figure 2. (**a**) N_2 adsorption–desorption isotherms and (**b**) the mesopore size distribution for the AHFS-treated and alkaline-treated USY.
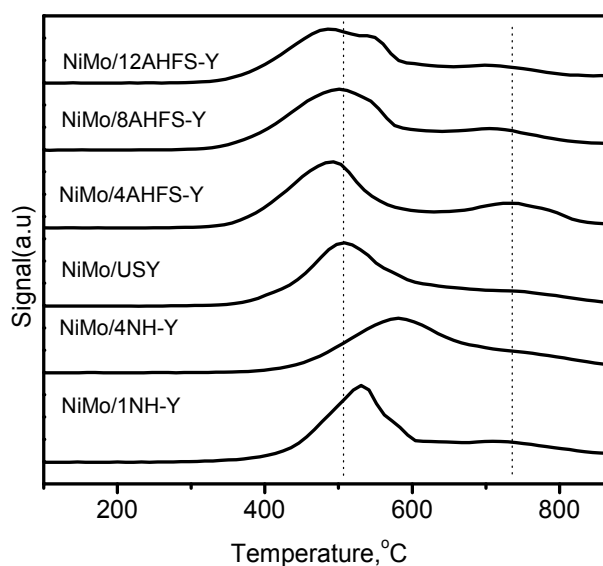
Table 3. The surface area and pore volume data of all the Y-type zeolites.

Samples	S_{micro} [a]	S_{ext} [b]	V_{micro} [c]	V_{meso} [d]	HF [e]
	m²/g	m²/g	cm³/g	cm³/g	
USY	609	49	0.28	0.07	0.0596
4AHFS-Y	598	57	0.28	0.10	0.0992
8AHFS-Y	381	92	0.18	0.17	0.1000
12AHFS-Y	196	106	0.09	0.29	0.0831
1NH-Y	618	48	0.29	0.07	0.0581
4NH-Y	551	101	0.26	0.10	0.1119

[a] t-plot micropore area. [b] t-plot external surface. [c] t-plot micropore volume. [d] Mesopore volume ($V_{total}-V_{micro}$), Vtotal is total pore volume test at p/p0 = 0.99. [e] The hierarchy factor (HF) = (V_{micro}/V_{pore}) × (S_{meso}/S_{BET}).

2.4. Influence of Dealumination and Desilication on the Metal State

The influence of AHFS or alkaline treatment on the active phase was investigated by hydrogen temperature-programmed reduction (H_2-TPR). As shown in Figure 3, the desilicated and dealuminated catalysts showed two principal reduction peaks. The low temperature peak around 500 °C was very broad and more intense, associated to the reduction of Mo^{6+} to Mo^{4+} of polymeric octahedral Mo species and $NiMoO_4^-$-like phase weakly bound to the zeolite surface [31,32]. The reduction peak at about 730 °C was assigned to the reduction of tetrahedrally coordinated Mo species (MoO_3 phase) in the zeolite cavities [33,34]. After AHFS treatments, the peak at ca. 500 °C gradually dissociated into two peaks, respectively assigned to the reduction of polymeric octahedral Mo species and $NiMoO_4^-$-like phase. The peak temperature for the polymeric octahedral Mo species shifted to the lower but the peak temperature for $NiMoO_4^-$-like phase shifted toward higher. Moreover, the intensity and area of the peak around 500 °C significantly increased and the peak intensity for MoO_3 phase also increase a little as the AHFS concentration increased. These suggested that large amount of Mo species in $NiMoO_4^-$ and MoO_3 phase were produced in the AHFS-treated catalysts. After alkaline treatments, the peak around 500 °C shifted to a higher temperature, but with a slight increase of the intensity and area as the alkaline concentration increased, suggesting that the proportion of $NiMoO_4^-$ phase increased with a little increase of the total metal active sites. These results indicated that the AHFS treated catalysts could better improve the dispersion of the active metal to produce more active sites than NaOH-treated catalysts. This was also further proved by CO chemisorption (see Table S1).

Figure 3. H_2-TPR profiles for NiMo catalysts supported on AHFS-treated USY and alkaline-treated USY.

2.5. Hydrotreating of Waste Cooking Oil

The desilicated and dealuminated USY supported sulphide NiMo catalysts showed high activity for the hydroconversion of WCO. The conversions of WCO were all most 100% for all the experiments. As shown in Figure 4, the yield of organic liquid products (Y_{OLP}) over the NaOH-treated catalysts were almost the same with that of USY, although the amount of strong acid sites of these catalysts was larger than USY. However, the Y_{OLP} increased with the severity increase of the AHFS treatment. The 82.3% yield of organic liquid products was obtained on the NiMo/8AHFS-Y catalyst. This indicated that the AHFS treatment could avoid excessive cracking to improve the yield of organic liquid products.
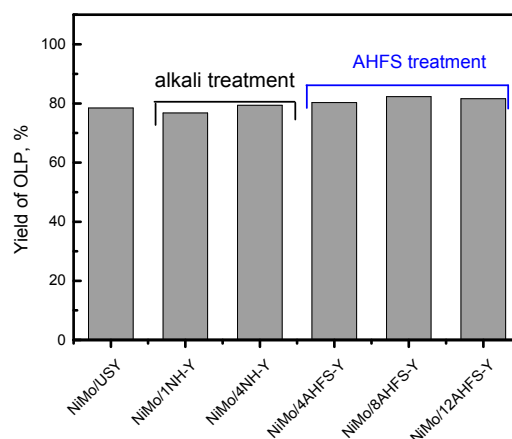

Figure 4. The yield of organic liquid product in the conversion of WCO over different catalysts.

The catalytic conversion of triglycerides to hydrocarbons proceeds through three reaction pathways, hydrodeoxygenation (HDO), decarbonylation (DCO), and decarboxylation (DCO_2) [9]. The decarbonylation (DCO) and decarboxylation (DCO_2) produced alkanes with one less carbon than the original fatty acid, but the same carbon atoms by hydrodeoxygenation (HDO). Thus, the molar ratio of C_{17}/C_{18} could reflect the tendency of DCOx/HDO reactions. Figure 5 shows the distribution of H_2O, CO, and CO_2 produced by different reaction pathways. The observed CO_2/CO ratios represented the relative rates of DCO_2/DCO ignoring the water-gas-shift reaction. From Figure 5b, the yield ratios of C_{17}/C_{18} increased for the AHFS treated catalysts and the $CO/(CO + CO_2)$ ratio was down to 0 under high AHFS concentration. This was in agreement with the results of the DCOx selectivity increasing with the increase of Si/Al ratio in the NiMo/SiO_2-Al_2O_3 catalysts [35]. In our previous research, we found that the Mo^{5+} and Mo^{6+} species mainly contributed to the DCOx reactions, especially the DCO_2 reaction, and Mo^{4+} favoured the HDO reaction. As shown in Figure 3, there were more Mo species in $NiMoO^{4-}$ and MoO_3 phase produced in the high AHFS-treated catalysts, which were generally accepted to be the active sites for DCO_2 reaction [36]. Therefore, the high selectivity of the DCO_2 reaction was achieved over the NiMo/8AHFS-Y and NiMo/12AHFS-Y catalysts. As for the NaOH-treated catalysts, the C_{17}/C_{18} ratio increased and the $CO/(CO + CO_2)$ ratio gradually decreased, indicating that the selectivity of DCOx, especially the DCO_2 reaction, was improved due to the increase of the $NiMoO^{4-}$ phase content. These results suggested that both the desilication and dealumination could enhance the selectivity of DCOx, especially DCO_2 reaction, in the hydroconversion of WCO. The dealumination with AHFS was a more efficient method to enhance the selectivity of DCO_2 reaction, and more than 67% DCOx selectivity (100% in DCO_2) reactions were achieved over high AHFS-treated catalysts.
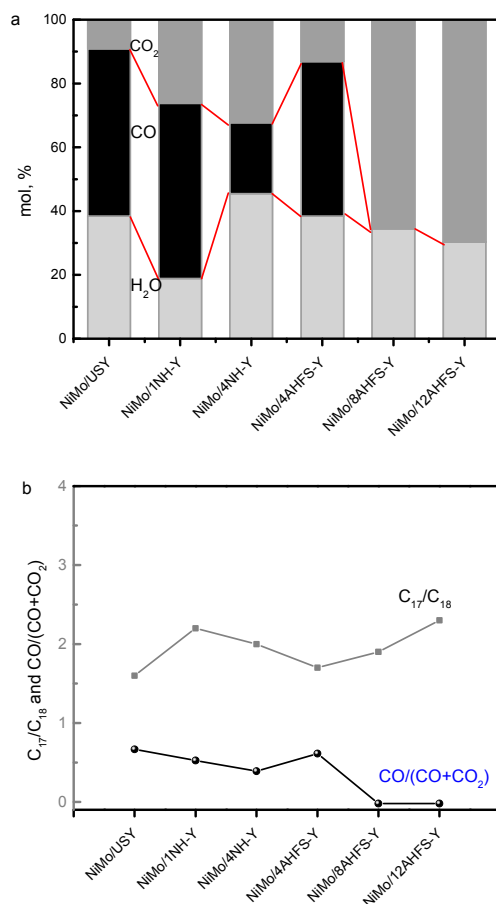
Figure 5. (**a**) Distribution of H_2O, CO, CO_2 products and (**b**) the variation of C_{17}/C_{18} and $CO/(CO + CO_2)$ in the conversion of WCO over different catalysts.

The products distributions were further analysed and summarized in Figure 6a. As for the AHFS-treated catalysts, it could be found that the selectivity of the gasoline-ranged hydrocarbons (C_4–C_8) decreased significantly compared with the NiMo/USY catalyst (from 76.6% to 52% for NiMo/4AHFS-Y) and further decreased to 30% (NiMo/8AHFS-Y) with the increase of the AHFS concentration. Meanwhile, the selectivity of jet fuel (C_9–C_{15} hydrocarbons) dramatically increased from 9.3% to 42.3% (NiMo/8AHFS-Y). The selectivity of diesel fraction (C_{16}–C_{18} hydrocarbons) also increased significantly (14.4% to 27.7%). This indicated that the cracking activity over the AHFS-treated catalysts decreased. It was possible that the deep cracking reaction was restrained by the decrease of the acid sites density, especially the Brønsted sited density. It should be noted that the NiMo/8AHFS-Y catalyst showed the suitable activity for selective cracking although the acid site density was very low. This might be attributed to the better acid distribution and mass transfer by the resulted hierarchical structure. While after low-concentration NaOH treatment, the NiMo/1NH-Y catalyst showed high selectivity of C_4–C_8 hydrocarbons (86.4%) due to the higher density of acid sites. However, after high concentration NaOH treatment, it was interested that although the acid sites density of NiMo/4NH-Y catalyst was much higher than NiMo/USY catalyst, the selectivity to the jet fuel fraction significantly increased to 29.7% with a relative low selectivity of C_4–C_8 hydrocarbons (47.3%). These results suggested that the selective cracking mainly depended on the location of acid sites, not the acid site density. The acid sites in the mesopore channel had better activity for selective hydroconversion of WCO than in the micropore and on the surface, and dealumination could produce a better hierarchical structure and acid distribution than desilicaton.
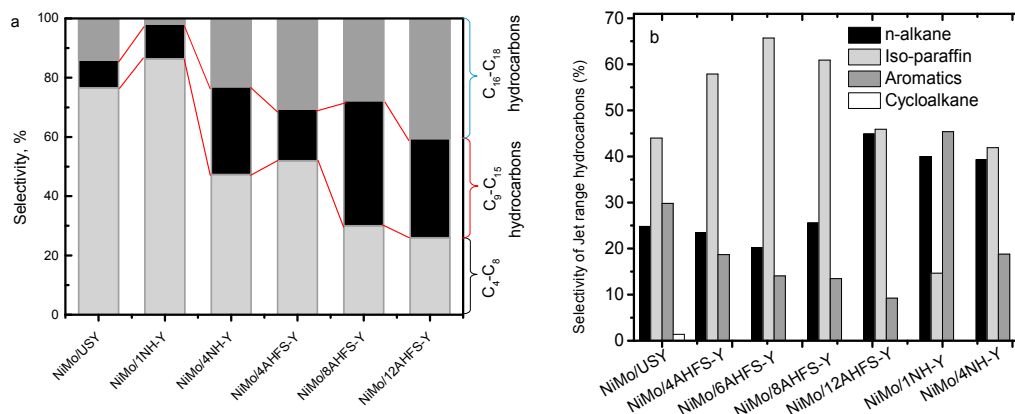
Figure 6. (**a**) The products distribution and (**b**) selectivity of various jet range hydrocarbon in the conversion of WCO over different catalysts.

Figure 6b shows the product distribution of C_{9-15} hydrocarbons over different catalysts. After mild AHFS treatment, the *iso-/n*-paraffins ratio (*i*/*n*) increased. The *i*/*n* ratios were 2.38, 2.47, and 3.25 corresponding to the ratio of the weak and strong acidity of 0.29, 0.47, and 0.56 (Table 2). After NaOH treatment, the *i*/*n* ratio decreased because of the stronger Brønsted acidity. Aromatic compounds were also produced besides paraffins. From Figure 6b the selectivity of jet-range aromatics (based on boiling point from C_9 to C_{15}) over the NiMo/AHFS-Y catalysts decreased with the increase of the AHFS concentration. This result indicated that the aromatization reaction of the cracking products was inhibited after AHFS treatment because of the decrease of the Brønsted and Lewis acidity. Recently, we found that the B/L ratio also played an important role in aromatization of olefins [36]. After AHFS treatment, the similar B/L ratio was obtained but the amount of these acid sites decreased significantly. Comparing to the NiMo/USY catalyst, the selectivity for jet-range aromatics over the NiMo/8AHFS-Y catalyst decreased about only by half (29.8% to 13.5%) although the amount of Brønsted and Lewis acid for the NiMo/USY catalyst was about 10 times as high as that for the NiMo/8AHFS-Y catalyst. Moreover the trimethylbenzene and methyl ethylbenzene in the aromatics increased because the proportion increase of stronger acid sites favoured the dealkylation of the higher aromatics with the increase of the AHFS concentration [37]. The selectivity of jet range aromatic hydrocarbons over NiMo/1NH-Y increased because of the density increase of strong Brønsted and Lewis sites. However, the selectivity of aromatic hydrocarbons over NiMo/4NH-Y decreased, probably due to the mismatching the B/L ratio and the enhancement of mass transfer by the mesopores. These results further indicated the importance of the B/L ratio for aromatization in hydroconversion of triglycerides.

2.6. Stability of Catalysts

The production of coke was the result of the formation of heavy compounds, which may cover certain acid sites and cause a hindrance to diffusion or block the channels of the catalyst and change the cracking activity [38]. The amount of coke was determined by TG in air. Figure 7 shows the observed mass losses for used catalysts after reaction for 7 h. As shown in Figure 7b, four stages of the mass loss from 30 °C to 230 °C, 230 °C to 330 °C, 330 °C to 520 °C, and 520 °C to 700 °C were observed which corresponded to the loss of adsorbed water, the formed soft coke, hard coke, and graphite, respectively [39]. The mass loss from 230 °C to 700 °C for used NoMo/USY, NiMo/4AHFS-Y, NiMo/6AHFS-Y, NiMo/8AHFS-Y, NiMo/1NH-Y, and NiMo/4NH-Y catalysts were 22.78%, 22.52%, 15.62%, 7.91% ,16.23%, and 15.34%, respectively. The total coke of used NiMo/AHFS-Y catalysts decreased with the increase in AHFS treatment severity. There were two likely reasons: Firstly, the number of acid sites, especially the strong acid sites, were mainly responsible for the coke deposition [40]. From Table 2, the AHFS-Y zeolites had a drastically lower acid amount than the corresponding USY zeolites and the acid amount decreased with the increase in AHFS treatment

severity. Secondly, the macromolecules would form in the free cavities of USY, and hard coke essentially located in the zeolite cavities and was difficult to diffuse out from the channel. From Table 3, the volume and the size of mesopores of AHFS treated USY increased, which would reduce the chance of the coke formation [41]. Although the number of strong acid sites increased for the alkaline treated USY, the volume of mesopores also increased, which reduced the coke.
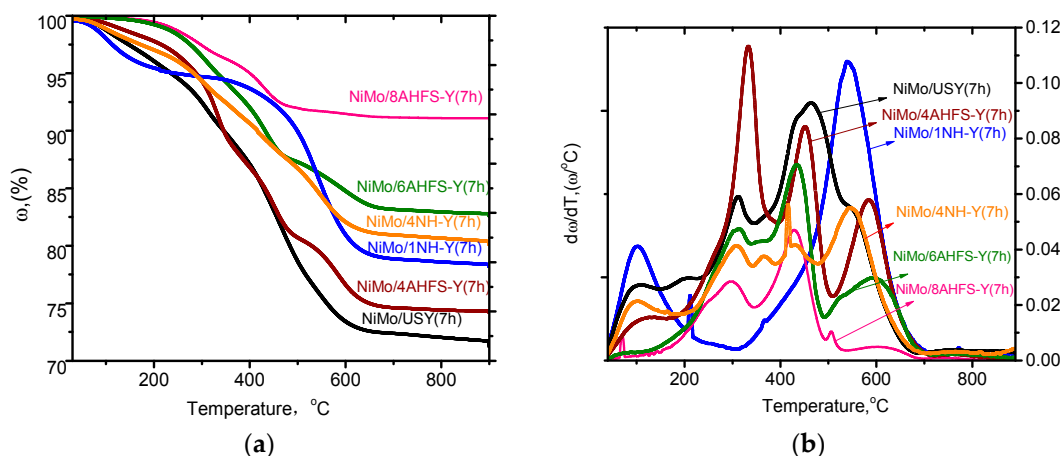

Figure 7. (**a**) TG and (**b**) DTG profiles for used NiMo/USY, NiMo/AHFS-Y, and NiMo/NH-Y catalysts.

3. Experimental

3.1. Materials

Commercial USY zeolite was purchased from Nankai University Catalyst Co. (Tianjin, China). $(NH_4)_6Mo_7O_{24}$ (≥99 wt %, J&K Chemical Ltd., Beijing, China), $Ni(NO_3)_2$ (≥98 wt %, Alfa Aesar, Shanghai, China), cyclohexane, ammonium nitrate (NH_4NO_3), ammonium hexafluorosilicate $(NH_4)_2SiF_6$ (≥98 wt %), and sodium hydroxide (NaOH) were purchased fromTianjin Guangfu Chemical Industry (Tianjin, China). The waste cooking oil was supplied by Tianjin Bihai Environmental Protection Ltd., Co., (Tianjin, China), which consisted of a mixture of used cooking oil mainly collected from local restaurants after being used for frying. WCO was filtered by a regular sieve to remove the remaining food particles before used as feedstock. The main physical and chemical properties of WCO are listed in Table 4.

Table 4. Physical and chemical properties of waste cooking oil.

Property	Waste Cooking Oil
Palimitic acid ($C_{16:0}$, wt %)	25.02
Linoleic acid ($C_{18:2}$, wt %)	28.85
Oleic acid ($C_{18:1}$, wt %)	39.69
Stearic acid ($C_{18:0}$, wt %)	6.27
Other acid (wt %)	0.17
Acid value (mg KOH^{-1})	65.47

3.2. Catalyst Preparation

3.2.1. Alkaline Treatment

In a typical run, USY powders were added into NaOH aqueous solution with different concentrations (1 wt %, 4 wt %). The mixture was heated to 363 K and stirred for 1 h in an oil bath. The slurry was filtered and washed with hot deionized water until neutral. Then, the obtained catalyst was dried at 393 K for 12 h and was converted into the H-type by three ion-exchanges (10 g sample in 100 mL

of 0.5 M NH_4NO_3). Before the third exchange, the sample was calcined at 823 K for 5 h for the Na^+ immigration from the β-cage to the supercage. Finally, the resultant samples were dried at 393 K overnight and calcined at 823 K for 5 h. The samples were denoted as 1NH-Y and 4NH-Y, respectively.

3.2.2. AHFS Treatment

The dealumination of USY was carried out in AHFS solutions according to the method in [25]. Ten grams of USY was suspended in 100 g distilled water and heated to 338 K, then an appropriate amount of AHFS with varying concentrations (4, 8, and 12 wt %) was added dropwise. The slurry was stirred at 338 K for 3 h. Then the zeolites were recovered by filtration and washed using deionized water to neutral. Samples were dried at 393 K for 12 h and calcined at 823 K for 5 h. The obtained samples were denoted as 4AHFS-Y, 8AHFS-Y, and 12AHFS-Y respectively.

3.2.3. Preparation of NiMo/Hierarchical USY

Ni (4.0 wt %) and Mo (12 wt %) were loaded on hierarchical USY by incipient wetness co-impregnation with the $(NH_4)_6Mo_7O_{24}$ and $Ni(NO_3)_2$ aqueous solution. After impregnation, the samples were kept overnight at room temperature, dried at 393 K for 12 h, and finally calcined at 823 K for 4 h.

3.3. Characterizations

XRD measurements were performed by using a D/MAX-2500 X-ray diffractometer with (Cu-Kα) radiation at 40 kV and 140 mA. The patterns were recorded in the 2θ range from 5° to 60° at a scanning rate of 2°/min. The framework Si/Al ratios of USY zeolites were estimated by Equation (1) [42]. The relative crystallinity was calculated by comparing the total peak intensities of (311), (331), (440), (533), (642), and (555) reflections between the treated samples and USY sample. The bulk Si/Al ratio of the zeolites was determined by an S4 PIONEER X-ray fluorescence (XRF) spectrometer.

$$\text{Framework Si/Al ratio} = (25.858 - \alpha)/(\alpha - 24.191) \tag{1}$$

where $\alpha = 6.671/\sin\theta$, the zeolites (2θ) were determined from the position of the (555) reflection.

Ammonia temperature programmed desorption (NH_3-TPD) was conducted on a chemisorption physisorption analyser (AMI-300, Altamira Instruments, Pittsburgh, PA., USA) equipped with a thermal conductivity detector (TCD). For the NH_3-TPD analysis, the samples were pretreated at 773 K in He for 1 h. After the samples cooled to 353 K, NH_3 adsorption was carried out by NH_3 in He at 393 K for 30 min. The NH_3-TPD profile was recorded from 393 K to 973 K after removing weakly adsorbed NH_3 by purging with He at 393 K for 2 h.

Py-FTIR measurement were carried out on a Bruker Vertex 70 FTIR spectrometer with a resolution of 4 cm^{-1}. 10 mg of the samples was pressed into a 13-mm-diameter self-supporting wafer and then was placed into the IR cell with CaF_2 windows. All samples were pre-treated under vacuum at 673 K for 1 h before Py-FTIR measurement. The background was recorded prior to adsorption experiments after the samples were cooled to 200 °C. Pyridine was injected into the cell and then was left in flowing N_2 for 30 min to allow the physisorbed pyridine to be desorbed. Spectra were recorded in the range of 1300 to 4000 cm^{-1}. The specific surface areas and pore volumes and pore size distribution of the samples were determined by N_2 adsorption-desorption isotherms on a Micromeritics ASAP-2020 apparatus. Before analysis, all samples were outgassed at 573 K for 4 h.

H_2-TPR experiments were conducted to determine the metal-support interaction and the metal dispersion. Before measurement, the samples were pretreated at 723 K in He for 1 h and cooled to room temperature. The reduction step was performed with a mixture of 10% H_2 in He, with a heating rate of 10 K/min, up to 1173 K. In the CO chemisorption experiments, the sample (100 mg) was pretreated in helium at 393 K for 1 h. Subsequently the sample was reduced in H_2 flow (50 cm^3/min) at 723 K for 2 h and then evacuated at 723 K for 2 h. Finally the sample was cooled to 313 K in vacuum.

Afterward the CO adsorption isotherm was recorded at 313 K based on the amount of adsorbed CO at different pressures.

3.4. Hydrotreating of Waste Cooking Oil

The hydroconversion of WCO was carried out in a fixed-bed flow reactor (1.2 cm I.D. and 45 cm in length). The reaction temperature was monitored with a thermocouple in the catalyst bed. Eight grams of the catalyst were diluted by SiC to obtain sufficient catalyst-bed length and was loaded into the steel reactor. WCO (20 wt %) in cyclohexane was used as the feedstock and supplied at a flow of 0.8 mL/min. The reactions were conducted at 380 °C under 3 MPa with H_2/Oil ratio (mL/mL) was 500. The catalysts were presulfided in situ at 320 °C and 3.0 MPa for 4 h using 3.0 wt % CS_2 in cyclohexane.

After the reaction reached stable (at least 5 h), the products were collected and were separated into gaseous products and the liquid products by a separator. The gaseous products were analysed by an Agilent Micro 3000 gas chromatograph equipped with three columns (molecular sieve, plot U, and alumina) and TCD detectors. The liquid fraction was separated into water and organic liquid products (OLPs). The water was weighted. The organic liquid products were qualitatively determined with an Agilent 6890N gas chromatography/5975N mass spectrometry (GC/MS). The hydrocarbons were quantitatively determined with a gas chromatographs (Bruker 456 GC, Bruker, San Francisco, CA, USA), equipped with a flame ionization detector (FID) and a commercially column (ZB-5 HT, 60 m × 0.25 mm × 0.25 μm). The conversion and selectivity were calculated by Equations (2)–(4):

$$\text{Conversion} = 100\% \times (\text{Feed}_G - \text{Product}_G)/\text{Feed}_G \tag{2}$$

$$\text{Selectivity}_{(CxHy)} = (\text{CH})_{\text{nproducts}}/\Sigma(\text{CH})_{\text{nproducts}} \tag{3}$$

$$\text{Selectivity of aromatics} = \Sigma(\text{CH})_{\text{aromatics}}/\Sigma(\text{CH})_{\text{nproducts}} \tag{4}$$

4. Conclusions

The hydrotreatment of waste cooking oil into a bio-jet fuel fraction was enhanced over the desilicated and dealuminated USY-supported sulfided NiMo catalysts. After desilicaton and dealumination, the mesopores with different inner surface structure were formed. The desilicated USY zeolite formed a high density of Brønsted acid sites. However, the dealuminated catalysts produced a low-acidity distribution and much larger mesopores than the dealuminated catalyst. The Brønsted acidity decreased in the AHFS treatment. A large amount of Mo species in $NiMoO_4^-$ and MoO_3 phases were produced in the AHFS-treated catalysts, while much more high-valence-state Mo species in the $NiMoO_4^-$ phase was formed over the NaOH-treated catalysts. Therefore, the catalysts modified by desilication and dealumination could enhance the selectivity of DCOx reactions. The AHFS-treated catalysts showed higher catalytic activity, prone to DCO_2 selectivity and better selective cracking for jet fuel.

References

1.　Rye, L.; Blakey, S.; Wilson, C.W. Sustainability of supply or the planet: A review of potential drop-in alternative aviation fuels. *Energy Environ. Sci.* **2010**, *3*, 17–27. [CrossRef]

2.　Kon, K.; Onodera, W.; Shimizu, K.I. Selective hydrogenation of levulinic acid to valeric acid and valeric biofuels by a Pt/HMFI catalyst. *Catal. Sci. Technol.* **2014**, *4*, 3227–3234. [CrossRef]

3.　Horacek, J.; Homola, F.; Kubickova, I. Lignin to liquids over sulfided catalysts. *Catal. Today* **2012**, *179*, 191–198. [CrossRef]

4.　Stumborg, M.; Wong, A.; Hogan, E. Hydroprocessed vegetable oils for diesel fuel improvement. *Bioresour. Technol.* **1996**, *56*, 13–18. [CrossRef]

5.　Sandor, K.; Tamas, K.; Artur, T. Fuel production by hydrotreating of triglycerides on NiMo/Al$_2$O$_3$/F catalyst. *Chem. Eng. J.* **2011**, *176*, 237–243.

6.　Satyarthi, J.K.; Chiranjeevi, T.; Gokak, D.T.; Viswanathan, P.S. An overview of catalytic conversion of vegetable oils/fats into middle distillates. *Catal. Sci. Technol.* **2013**, *3*, 70–80. [CrossRef]

7.　Perego, C.; Ricci, M. Diesel fuel from biomass. *Catal. Sci. Technol.* **2012**, *2*, 1776–1786. [CrossRef]

8.　Yang, Y.; Wang, Q.; Zhang, X.; Wang, L.; Li, G. Hydrotreating of C18 fatty acids to hydrocarbons on sulphided NiW/SiO$_2$-Al$_2$O$_3$. *Fuel Process. Technol.* **2013**, *116*, 165–174. [CrossRef]

9.　Bezergianni, S.; Kalogianni, A. Hydrocracking of used cooking oil for biofuels production. *Bioresour. Technol.* **2009**, *100*, 3927–3932. [CrossRef] [PubMed]

10.　Rogelio, S.B.; Fernando, T.Z.; Felipe, J.H.L. Hydroconversion of Triglycerides into Green Liquid Fuels. In *Hydrogenation*; Karamé, I., Ed.; InTech: Rijeka, Croatia, 2012; pp. 188–216.

11.　Honeywell UOP, Honeywell Green Jet Fuel. Available online: http://www.uop.com/processing-solutions/renewables/green-jet-fuel/#uop-renewable-jet-fuel-process (accessed on 20 October 2016).

12.　Verma, D.; Kumar, R.; Rana, B.S.; Sinha, A.K. Aviation fuel production from lipids by a single-step route using hierarchical mesoporous zeolites. *Energy Environ. Sci.* **2011**, *4*, 1667–1671. [CrossRef]

13.　Verma, D.; Rana, B.S.; Kumar, R.; Sibi, M.G.; Sinha, A.K. Diesel and aviation kerosene with desired aromatics from hydroprocessing of jatropha oil over hydrogenation catalysts supported on hierarchical mesoporous SAPO-11. *Appl. Catal. A Gen.* **2015**, *490*, 108–116. [CrossRef]

14.　Rocha Filho, G.N.; Brodzki, D.; Djega-Mariadassou, G. Formation of alkanes, alkylcycloalkanes and alkylbenzenes during the catalytic hydrocracking of vegetable oils. *Fuel* **1993**, *72*, 543–549. [CrossRef]

15.　Morais, S.; Mata, T.M.; Martins, A.A.; Pinto, G.A.; Costa, C.A.V. Simulation and life cycle assessment of process design alternatives for biodiesel production from waste vegetable oils. *J. Clean. Prod.* **2010**, *18*, 1251–1259. [CrossRef]

16.　Chiaramonti, D.; Prussi, M.; Buffi, M.; Tacconi, D. Sustainable bio kerosene: Process routes and industrial demonstration activities in aviation biofuels. *Appl. Energy* **2014**, *136*, 767–774. [CrossRef]

17.　Talebian-Ki akalaieha, A.; Amina, N.A.S.; Mazaheria, H. A review on novel processes of biodiesel production from waste cooking oil. *Appl. Energy* **2013**, *104*, 683–710. [CrossRef]

18.　Yaakob, Z.; Mohammad, M.; Alherbawi, M.; Alam, Z.; Sopian, K. Overview of the production of biodiesel from Waste cooking oil. *Renew. Sustain. Energy Rev.* **2013**, *18*, 184–193. [CrossRef]

19.　Li, T.; Cheng, J.; Huang, R.; Zhou, J.; Cen, K. Conversion of waste cooking oil to jet biofuel with nickel-based mesoporous zeolite Y catalyst. *Bioresour. Technol.* **2015**, *197*, 289–294. [CrossRef] [PubMed]

20.　Liu, S.; Zhu, Q.; Guan, Q.; He, L.; Li, W. Bio-aviation fuel production from hydroprocessing castor oil promoted by the nickel-based bifunctional catalyst. *Bioresour. Technol.* **2015**, *183*, 93–100. [CrossRef] [PubMed]

21.　Garralon, G.; Fornes, V.; Corma, A. Faujasites dealuminated with ammonium hexafluorosilicate: Variables affecting the method of preparation. *Zeolites* **1988**, *8*, 268–272. [CrossRef]

22.　Silaghi, M.C.; Chizallet, C.; Raybaud, P. Challenges on molecular aspects of dealumination and desilication of zeolites. *Microporous Mesoporous Mater.* **2014**, *191*, 82–96. [CrossRef]

23.　Verboekend, D.; Nuttens, N.; Locus, R.; Van Aelst, J.; Verolme, P.; Groen, J.C.; Pérez-Ramírez, J.; Selsa, B.F. Synthesis, characterisation, and catalytic evaluation of hierarchical faujasite zeolites: Milestones, challenges, and future directions. *Chem. Soc. Rev.* **2016**, *45*, 3331–3352. [CrossRef] [PubMed]

24. Huang, S.; Chen, P.Z.; Yan, B.; Wang, S.; Shen, Y.; Ma, X. Modification of Y Zeolite with Alkaline Treatment: Textural Properties and Catalytic Activity for Diethyl Carbonate Synthesis. *Ind. Eng. Chem. Res.* **2013**, *52*, 6349–6356. [CrossRef]

25. Qin, Z.; Shen, B.; Gao, X.; Lin, F.; Wang, B.; Xu, C. Mesoporous Y zeolite with homogeneous aluminum distribution obtained by sequential desilication–dealumination and its performance in the catalytic cracking of cumene and 1,3,5-triisopropylbenzen. *J. Catal.* **2011**, *278*, 266–275. [CrossRef]

26. Qin, Z.; Shen, B.; Yu, Z.W.; Deng, F.; Zhao, L.; Zhou, S.; Yuan, D.; Gao, X.; Wang, B.; Zhao, H.; et al. A defect-based strategy for the preparation of mesoporous zeolite Y for high-performance catalytic cracking. *J. Catal.* **2013**, *298*, 102–111. [CrossRef]

27. Donk, S.; Janssen, A.H.; Bitter, J.H. Generation, Characterization, and Impact of Mesopores in Zeolite Catalysts. *Catal. Rev.* **2003**, *45*, 297–319. [CrossRef]

28. Corma, A.; Fornes, V.; Rey, F. Extraction of extra-framework aluminium in ultrastable Y zeolites by $(NH_4)_2SiF_6$ treatments: I. Physicochemical Characterization. *Appl. Catal.* **1990**, *37*, 267–274. [CrossRef]

29. Xu, B.; Bordiga, S.; Prins, R.; Van Bokhoven, J.A. Effect of framework Si/Al ratio and extra-framework aluminum on the catalytic activity of Y zeolite. *Appl. Catal. A Gen.* **2007**, *333*, 245–253. [CrossRef]

30. Peng, X.; Zhang, Y.Z.; Zheng, L.B. Isomorphous subsitution of Faujusite with $(NH_4)_2SiF_6$: Reaction conditions and properties of products. *J. Catal.* **1991**, *13*, 32–37.

31. Peng, X.; Zhang, Y.; Zheng, L.B. Isomorphous subsitution of Faujusite with $(NH_4)_2SiF_6$: Reaction mechanism. *J. Catal.* **1993**, *14*, 300–306.

32. Cordero, R.L.; Agudo, A.L. Effect of water extraction on the surface properties of Mo/Al_2O_3 and $NiMo/Al_2O_3$ hydrotreating catalysts. *Appl. Catal. A Gen.* **2000**, *202*, 23–35. [CrossRef]

33. Cordero, R.L.; Llambias, F.J.G.; Agudo, A.L. Temperature-programmed reduction and zeta potential studies of the structure of MoO_3/Al_2O_3 andMoO_3/SiO_2 catalysts effect of the impregnation pH and molybdenum loading. *Appl. Catal.* **1991**, *74*, 125–136. [CrossRef]

34. Solis, D.; Agudo, A.L.; Ramírez, J.; Klimova, T. Hydrodesulfurization of hindered dibenzothiophenes on bifunctional NiMo catalysts supported on zeolite–alumina composites. *Catal. Today* **2006**, *116*, 469–477. [CrossRef]

35. Gong, S.; Shinozaki, A.; Qian, E.W. Role of Support in Hydrotreatment of Jatropha Oil over Sulfided NiMo Catalysts. *Ind. Eng. Chem. Res.* **2012**, *51*, 13953–13960. [CrossRef]

36. Chen, H.; Wang, Q.; Zhang, X.; Wang, L. Quantitative conversion of triglycerides to hydrocarbons over hierarchical ZSM-5 catalyst. *Appl. Catal. B Environ.* **2015**, *166–167*, 327–334. [CrossRef]

37. Adjaye, J.D.; Katikaneni, S.P.R.; Bakhshi, N.N. Catalytic conversion of a biofuel to hydrocarbons: Effect of mixtures of HZSM-5 and silica-alumina catalysts on product distribution. *Fuel Process. Technol.* **1996**, *48*, 115–143. [CrossRef]

38. Liu, X.J.; Guan, L.L.; Fu, X.N.; Zhao, Y.; Wu, J.D.; Xu, N. Nanocone arrays synthesized by plasma-assisted reaction deposition. *Nanoscale Res. Lett.* **2014**, *9*, 550. [CrossRef] [PubMed]

39. Li, Y.; Zhang, C.S.; Liu, Y.G.; Hou, X.; Zhang, R.; Tang, X. Coke Deposition on Ni/HZSM-5 in Bio-oil Hydrodeoxygenation Processing. *Energy Fuels.* **2015**, *29*, 1722–1728. [CrossRef]

40. Silva, A.O.S.; Souza, M.J.B.; Aquino, J.M.F.B.; Fernandes, V.J., Jr.; Araujo, A.S. Acid properties of the HZSM-12 zeolite with different Si/Al ratio by thermo-programmed desorption. *J. Therm. Anal. Calorim.* **2004**, *76*, 783–791. [CrossRef]

41. Liu, J.X.; Cai, G.; Yang, L.X.; Gao, X.-Y.; Ji, P.; Chen, G.-Q. The coking behaviour of zeolife catalysts during the conversion of methanol to lower olefins. *J. Catal.* **1985**, *6*, 238–244.

42. Breck, D.W.; Flanigen, E.M. *Molecular Sieves*; Society of Chemical: London, UK, 1968.